Preparation of highly emissive and reproducible Cu−In−S/ZnS core/shell quantum dots with a mid-gap emission character

Nawzad Nadhim Jawhar [a, b], Ehsan Soheyli [c, ***], Ahmet Faruk Yazici [d], Evren Mutlugun [e, **], Reza Sahraei [a, *]

[a] Department of Chemistry, Faculty of Science, Ilam University, 65315-516, Ilam, Iran
[b] Department of Chemistry, College of Education, University of Garmian, 46021, Kalar, Iraq
[c] Department of Physics, Faculty of Science, Ilam University, 65315-516, Ilam, Iran
[d] Department of Material Science and Nanotechnology Engineering, Abdullah Gul University, Kayseri, 38080, Turkey
[e] Department of Electrical-Electronics Engineering, Abdullah Gul University, Kayseri, 38080, Turkey

ARTICLE INFO

ABSTRACT

Copper indium sulfide (CIS) quantum dots (QDs) are one of the newest types of luminescent semiconductors with low-toxicity and earth-abundant features. The present work reports the successful aqueous synthesis of CIS/ZnS core/shell QDs using dual-stabilizing agents of N-acetyl-ʟ-cysteine and trisodium citrate. Off-stoichiometric QDs with In-rich compositions were found to be very small and highly emissive after coating by a shell of wide bandgap ZnS. The effect of various experimental parameters was evaluated to achieve highly reproducible QDs with bright reddish emission. Results showed a significant contribution of mid-gap defect states in the recombination processes (based on the gradual increase in absorbance recorded for samples, relatively high Urbach energy, large Stokes shift, large FWHM value in PL spectra, as well as the long-lived PL decay time). In addition, the chemical stability of samples was investigated using highly oxidant H_2O_2 agent and results demonstrate their superior stability. The combination of low-toxicity, intense and stable emission, along with synthetic advantages demonstrates that the present aqueous-soluble and emissive QDs can be considered as an excellent bio-photonic structure suitable for different fields of biological imaging and diagnostics.

© 2020 Elsevier B.V. All rights reserved.

1. Introduction

As colloidal semiconductor materials, QDs have introduced themselves as technologically utilizable sort of nanoscale structures with unique optical properties, ease of preparation and control. One of the main constraints on the development of QDs in many technologies is the unavailability of non-toxic materials with appropriate properties and performance. Ternary I−III−VI type semiconductor QDs with the various chemical compositions are the new frontier for conventional heavy metal-containing QDs [1]. Among them, copper indium sulfide (CIS) structures with direct bandgap energy in the bulk of 1.45 eV are very important for many applications in modern technologies [2]. The combination of structural-driven optical merit and biological safety introduces them as technologically favorable QDs for potential applications in biophotonics [1], photoelectrochemical water splitting [3], photocatalysis [4], solar cell [5], and white light-emitting diodes [6]. Previous studies have revealed that the intrinsic crystal defects or internal defects associated with CIS semiconductors are attributed to their off-stoichiometric properties [7−10]. They can comprise a large density of non-stoichiometric ions, rather than their II-VI counterparts. Indeed, the diverse anti-sites (In_{Cu}, Cu_{In}), interstitial sites (Cu_i, In_i) or vacancies (V_{Cu}, V_{In}, V_S) are probable defects created in such structures. These defects would be remarkably effective on optical characteristics of CIS QDs, and especially the way in which photoluminescence (PL) processes occur. Chen et al. have attributed the PL emission peak of the off-stoichiometry $CuInS_2$/ZnS QDs to the transformation of photon-generated excitons to donor-acceptor pair (DAP) states as V_{cu} and In_{cu} sites [11]. Klimov's group exhibited direct pieces of evidence on the key role of Cu-deficient defect states as intra-gap emission centers for CIS

* Corresponding author.
** Corresponding author.
*** Corresponding author.
    E-mail addresses: ehs.soheyli@gmail.com (E. Soheyli), evren.mutlugun@agu.edu.tr (E. Mutlugun), r.sahraei@ilam.ac.ir (R. Sahraei).

QDs [10]. Therefore, offering a simple method to synthesize such superior emissive QDs is of great interest especially using an environmentally benign aqueous-based method, because in many potential applications of ternary QDs, in particular, as luminescent biomarkers or sensors, they are required to be soluble in polar solvents such as water [12]. Up to now, various techniques with different stabilizers have been employed for the straightforward synthesize of hydrophilic CIS QDs such as reflux [13], hydrothermal [14] and microwave-assisted approaches [15]. On the other hand, in order to enhance their stability in aqueous solution over wide ranges of pH and ionic strength, the surface of QDs should be modified. This surface modification will lead to maintaining/protecting the optical properties of QDs, as well as generating the functional groups that facilitate the strong conjugation of the QD surface into proteins, antibodies, aptamers, and oligonucleotides. In this regard, potent organic molecules such as L-glutathione [16], and 3-mercaptopropionic acid (3-MPA) [13] have been used for preparing CIS QDs. Zhang et al. examined several short-chain thiols involving 3-MPA, mercaptosuccinic acid, L-cysteine, thioglycolic acid (TGA), and 1-thioglycerol, but they reported that only MPA and TGA were feasible to the synthesis of colloidal CuInS$_2$ QDs [17]. N-acetyl-L-cysteine (NAC) is another stabilizer molecule with a soft base character, which to the best of our knowledge has not been used for the preparation of CIS QDs so far. Nonetheless, a wide range of cations utilized in such I-III-VI- type QDs, and the difference in their chemical reactivity make it difficult to reach multicomponent QDs without any trace of compositional phase separation [8]. This is the property related to the acidic/basic nature of species. Therefore, to overcome this problem, it would be necessary to use second hard base stabilizer molecules to regulate the growth of QDs by complexing with cations [18]. In this regard, trisodium citrate can be an excellent stabilizer to compensate the stabilizing drawback that happens during the synthesis process of such multinary structures.

Another approach to improve the physicochemical properties of QDs is the covering of existing core QDs with an additional inorganic shell (with the wide bandgap energy and the minimized lattice mismatch) [19]. This additional shell can passivate the non-saturated surface states, confine the charge carriers in core structure, enhance the emission intensity, and improve their stability. ZnS can be a valuable choice as an additional shell due to its eco-friendly characteristics, wide-bandgap of E$_{g-bulk}$ = 3.6 eV, along with nearly similar lattice parameters to that of CIS core structure. Long et al. prepared CIS/ZnS nanocrystals with PL quantum yield of ~26% using glutathione and trisodium citrate (SC) as stabilizing agents and studied their biosensing potentials [20]. Pan's group reported an emission quantum yield up to 38% for CIS QDs upon ZnS shell coating through a facile way and at the co-presence of L-glutathione and sodium citrate [18]. In another report, Zhang et al. synthesized the 3-mercaptopropionic acid-capped ternary Cu−In−S (CIS) and quaternary Zn−Cu−In−S (ZCIS) QDs with different composition ratios via a facile aqueous route [13].

By the simultaneous utilization of NAC and SC (as soft and hard base species, respectively) in the present work, the highly water-soluble, emissive, stable, and off-stoichiometric CIS/ZnS QDs were successfully synthesized. It was found that experimental variables are highly effective on the optical characteristics of the QDs. Based on the results recorded, the considerable effect of the donor-acceptor mid-gap levels in both absorption and emission processes were observed. Regarding the simplicity of synthesis strategy, high emission intensity and stability, and low-toxicity of the as-prepared CIS/ZnS QDs, the present samples can be used for future biological applications including bio-imaging, cell-tracking, and even photocatalytic intentions.

2. Experimental section

2.1. Materials

Zn(CH$_3$COO)$_2$.2H$_2$O (Merck, ≥99%), Cu(NO$_3$)$_2$·3H$_2$O (Merck, 99.9%), In(NO$_3$)$_3$ (Merck, 99.99%), NAC (Merck, ≥99%), Na$_3$C$_6$H$_5$O$_7$ (trisodium citrate dehydrate, Merck, 99−101%), Na$_2$S.xH$_2$O (Across organics, 60−63%), CH$_4$N$_2$S (thiourea, Merck, 99%), NaOH (Merck, ≥99%), CH$_3$COCH$_3$ (acetone, Merck, ≥99.8%) were used as received. Deionized water was also used for all experiments.

2.2. Methods

Initial conditions in this experimentally one-pot/two-steps method were as follows. First, 75 μL of 1 M indium nitrate (in ethanol), 0.9 mL of 0.01 M copper nitrate (in water), 0.4 mL of 1 M sodium citrate (in water) and 8 mg NAC were dissolved in 20 mL double distilled water. The solution pH was adjusted to 8 (using 1 M sodium hydroxide). Then, the solution was transferred to a three-necked flask previously placed in an oil bath. After deaeration using nitrogen gas, 65 μL of 1 M sodium sulfide was added to stirring solution (fast injection at room temperature) and the heating process was started. Next, the reaction solution was refluxed for 45 min in a very weak nitrogen atmosphere and at a temperature of 100 °C. The PL emission measurement performed at this step demonstrated that the bare CIS QDs do not show any emission signal. After that, a specific amount of ZnS shell precursor solution (containing 190 mg NAC, 60 mg thiourea, and 170 mg Zn) was swiftly injected into the stirred solution and heated for extra 45 min. Finally, the solution was cooled down to the lab temperature. The optical measurements were carried out at this step. On the other hand, the precipitation process of the colloidal QDs was performed as follows; acetone was slowly added to the colloidal QDs until the solution becomes completely opaque. Then, the resulting colloidal solution was centrifuged at 4000 rpm to obtain QDs in a precipitate form. The resulting precipitate was dried at room temperature and used for further experiments. The starting feed ratio of precursors was In:Cu:NAC:SC:Na$_2$S = 1:0.12:0.7:5.4:0.8 in core solution and Zn:NAC:thiourea = 1:1.5:1 in ZnS shell solution. Aqueous-phase synthesis of QDs and the physical/chemical quality of the QDs is highly dependent on the experimental variables. Therefore, the various experimental parameters were optimized and their effects on optical characteristics of CIS/ZnS QDs were investigated.

2.3. Instruments

The light absorbance properties of the as-prepared QDs were measured by Cary 300 Bio UV−Vis spectrophotometer (VARIAN) at the wavelength range of 200−800 nm. The PL emission spectra of as-prepared QDs were recorded using a Cary Eclipse fluorescence spectrophotometer (Agilent technology). The crystallinity of synthesized particles was characterized using a Philips X'pert diffractometer in the 2θ range from 10° to 70°. The size and shape of the particles were observed under a FEI Talos F200S transmission electron microscope (TEM) at an operating voltage of 150 kV. The size and size distribution of the QDs were also measured by the dynamic laser light scattering (Zetasizer Nano series, Malvern Instruments Co.). The chemical composition and EDX-mapping of samples were obtained by an energy dispersive X-ray analysis (EDX) instrument (Oxford INCA II energy solid-state detector). Inductively coupled plasma atomic emission spectroscopy (ICP-AES; Varian Vista-Pro) was used to determine the exact composition of Cu-to-In molar ratio at the core/shell QDs. The time-resolved PL measurements were performed by PicoQuant

Fluo Time 200 time-correlated single-photon counting system equipped with a laser excitation source operating at 375 nm having a 50 kHz repetition rate. Lifetimes of the samples were collected with Time Harp 260 PICO system. The decay curves were modeled and amplitude average lifetimes were calculated by fitting the data with two exponentials using FluoFit software by PicoQuant Technologies. The calculation of PL emission efficiency was done based on our previous work [21]. In summary, the formula of $\{QY_{QDs} = QY_{ref} \times (I_{QDs}/I_{ref}) \times (OD_{ref}/OD_{QDs}) \times (n^2_{QDs}/n^2_{ref})\}$ was used, where I, OD and n refer to integrated emission intensity, absorption intensities at the excitation wavelength, and refractive index of the solvent, respectively. Fluorescein in 0.1 M NaOH was also used as a reference (QY = 0.79 at the excitation wavelength of 440 nm).

3. Results and discussion

3.1. EDX/EDX-mapping

The chemical composition of the QDs was determined by EDX and EDX-mapping analysis (Fig. 1). The presence of all expected species (In, Cu, S, and Zn) is confirmed in the EDX profile of CIS/ZnS QDs. This also approved in EDX-mapping images. However, as one can find out, the amount of indium atoms incorporated into the lattice structure of QDs is very larger than that of copper. This means that the present multicomponent samples are non-stoichiometric I-III-VI structures with In-rich composition. Such compositions are supposed to be better nano-emitters than those of stoichiometric or Cu-rich I-III-VI compositions [22].

3.2. XRD and TEM

The XRD pattern of CIS core and CIS/ZnS QDs prepared at a re-action temperature of 100 °C is shown in Fig. 2A. The standard XRD peak positions of CIS and ZnS were also provided at the bottom of the Figure. An overlap in the position of core and shell structures is obvious. Albeit, the XRD peaks are very broad, which are related to the nanoscale size of the synthesized QDs, it suggests that the resulting samples correspond to the tetragonal phase chalcopyrite of CIS structure (ICDD 85−1575). However, there is a slight shift in the pattern toward higher diffraction degrees which is related to the coating effect of the ZnS shell layer. As can be seen, the result is a multi-peak pattern with three broad peaks related to (112), (204)/(220), and (116)/(312) Miller indices for the CIS, which is well consistent with results reported by Chen et al. for In-rich composition [11] or (111), (220), and (311) planes of the cubic ZnS (JCPDS 36−1450). The peak located below 2θ = 25° is due to possible organics remains in powder samples even after purification [23]. Of course, it should be pointed out that since the pattern is very broad, it is difficult to determine exactly whether the crystal structure is tetragonal or cubic.

In order to achieve a direct observation of the shape, size, and uniformity of the samples, the TEM image of the CIS/ZnS QDs was obtained. As seen in Fig. 2B, the QDs are well-separated with a relatively spherical shape. These sizes are comparable to the Bohr exciton radius for the bulk chalcopyrite CIS (4.1 nm) [2], which indicates that the quantum confinement regime is effective on the charge carriers and optical properties of the core/shell QDs. The TEM image of typical CIS/ZnS core/shell QDs shows an almost clear lattice fringe with an interplanar spacing of 0.31 nm, which is quite similar to those reported for (112) lattice fringes in Cu−In−S and matching well with the (111) plane of cubic ZnS. This demonstrates the crystalline nature of core/shell QDs. Fig. 2C further supports the small size of as-prepared core/shell QDs and shows that upon an increase at refluxing temperature (60, 80, and 100 °C), the average size of QDs also increases (~4.5, 6.1, and 6.9 nm).

3.3. UV-Vis and PL emission spectra

The final goal of the present work was to prepare the emissive CIS-based QDs. However, the PL emission spectrum of the bare CIS QDs does not show any luminescence signal (see Fig. 3A and B). The surface defects-related nonradiative-recombination centers might be responsible for this observation. Therefore, a ZnS shell precursor solution was added to pre-existing CIS QDs. This lead to the formation of CIS/ZnS type-1 core/shell QDs with strong reddish
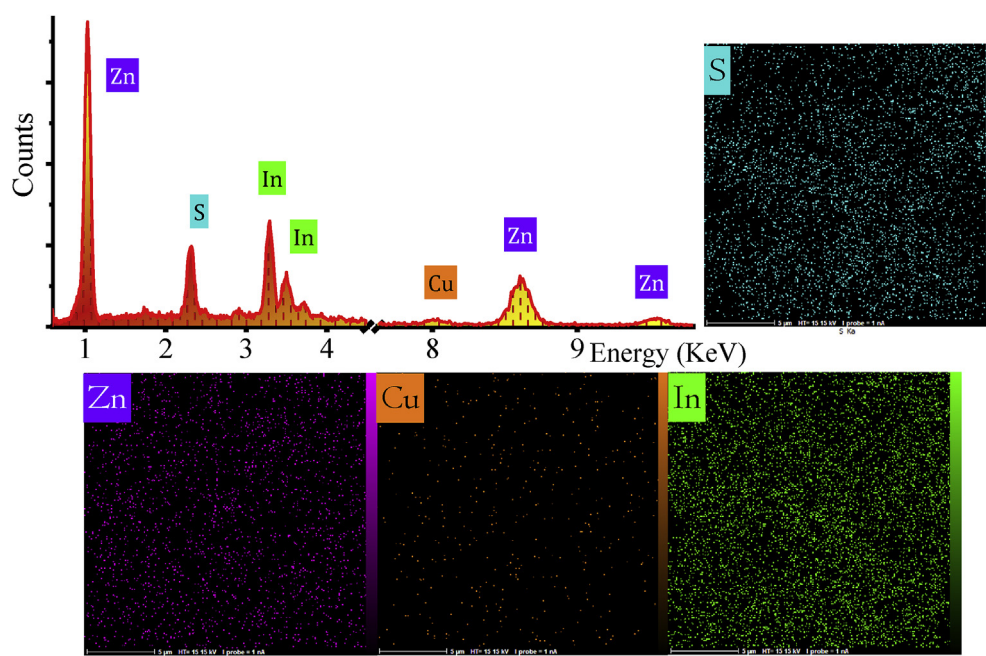

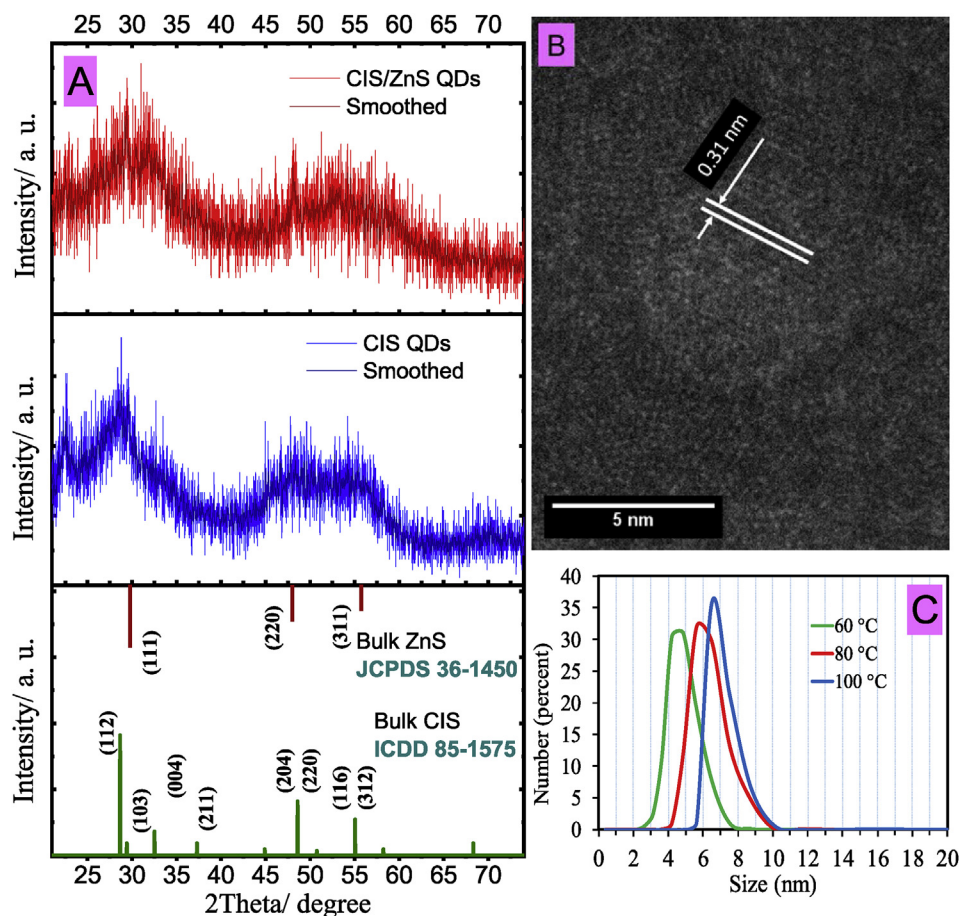**Fig. 1.** EDX, and EDX-mapping results for typical CIS/ZnS core/shell QDs.

Fig. 2. (A) XRD patterns of CIS and CIS/ZnS core/shell QDs, (B) TEM image of core/shell QDs and (C) zeta sizer measurements of CIS/ZnS core/shell QDs prepared at different reaction tempeartures.

emission. As can be observed in Fig. 3A and B, the strategy used here dramatically enhances the emission peak intensity by several hundred-fold at around 638 nm, which is of great interest from both fundamental and technological perspectives. The reason for this variation can be associated with a reduction in the nonradiative-recombination centers due to the successful elimination of surface trap states of CIS QDs by ZnS coating. Apart from this alteration, the nature of the luminescence process in CIS QDs is still under controversy. It has been proved that the dominant PL mechanisms in I-III-VI semiconducting structures widely differ from those happen for classical II-VI semiconductors [11,24]. While the second category has an excitonic-governing recombination mechanism, the first one shows a defect-governing PL attitude. Yan et al. have reported that the origin of the PL band emission located near 642 nm in CIS QDs is attributed to the donor-acceptor electron transitions [23]. The PL emission QY increased remarkably from 0 to ~18% upon the coating by ZnS shell.

As can be seen in Fig. 3, the full width at half maximum (FWHM) of the emission peak is about 125 nm (370 meV). This large FWHM value implies the key role of intra-gap levels in the recombination process. Most researchers have attributed these observations to the dynamics of electron-phonon interaction and vibrational relaxation [25]. However, Fuhr et al. believed that while electron-phonon coupling for QDs systems (with optically active Cu impurities) is stronger than typical II-VI QDs, the spectral broadening predominantly occurs due to the inhomogeneous spatial distribution of Cu impurities [26]. In order to further demonstrate the key role of mid-gap energy levels in the recombination process, the time-correlated

single-photon counting (TSCPC) decays of CIS/ZnS core/shell QDs prepared at different reaction temperatures were carried out (Fig. 3C) and results were given in Table 1. First, the relatively long-lived PL decay curves somehow indicate the contribution of midgap defect levels. Secondly; the multiexponential nature of all profiles revealed the presence of various radiative pathways. As illustrated above, the donor-acceptor pair and surface defect-involved recombinations are responsible for PL characteristics in such QDs. Hence, there might be a combined role of these levels. Finally, based on the emission kinetics recorded, the average lifetime increased from 45.1 ns to 127.7 ns as the reaction temperature increases from 60 °C to 100 °C. This observation is quite similar to those reported by others [27]. Despite the intrinsic donor/acceptor defects (which play a role of deep trap states), the surface-related defects lead to the formation of shallow energy levels which are known through their faster recombination lifetime. At a low temperature of 60 °C, the PL decay rate is 45.1 nm, which shows the remarkable contribution of surface-defect sites in the recombination of carriers. However, at higher temperatures, the donor-acceptor levels play a prominent role and therefore, the PL decay curve of core/shell QDs shows a prolonged time. This fully aligns with the experimental red shift of PL emission spectra in Fig. 4A. Therefore, the PL decays further support the effective role of mid-gap energy levels and especially the donor-acceptor levels in intense PL emission observed for as-prepared CIS/ZnS core/shell QDs.

3.3.1. Effect of reaction temperature

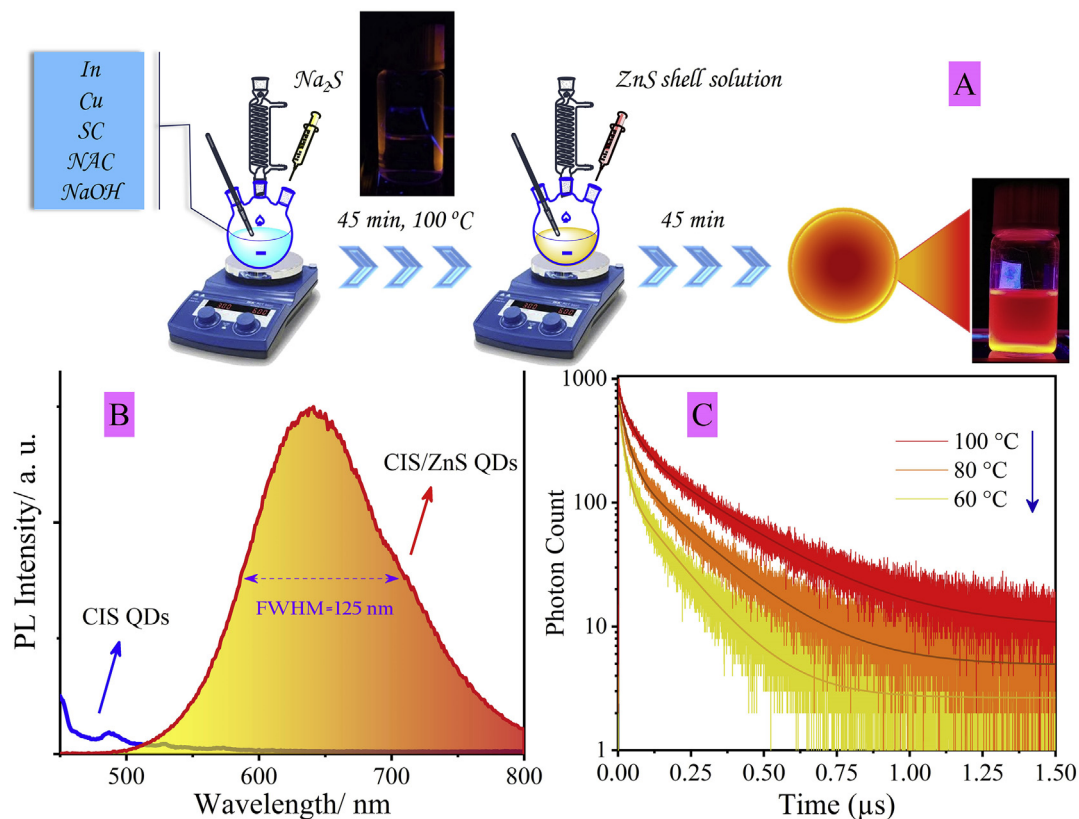Fig. 4A shows the absorption and PL emission spectra of CIS/ZnS

Fig. 3. (top) A schematic of the synthesis procedure at a temperature of 100 °C (the digital image of CIS and CIS/ZnS QDs under 365 nm UV irradiation are also shown). (Bottom) The PL spectra of bare CIS and CIS/ZnS QDs at the excitation wavelength of 365 nm and TSCPC decays of core/shell QDs at different reaction temperatures.

Table 1
The lifetime components of CIS/ZnS QDs prepared at different reaction temperatures.

	A_1	τ_1 (ns)	A_2	τ_2 (ns)	$\tau_{average}$ (ns) (amplitude)
60 °C	131.2 ± 6.85	143.3 ± 6.0	473.4 ± 40.3	17.9 ± 1.6	45.1
80 °C	191.0 ± 8.33	198.6 ± 6.8	473.2 ± 41.2	28.1 ± 2.7	77.1
100 °C	291.8 ± 8.95	263.9 ± 6.4	471.3 ± 36.8	43.5 ± 3.8	127.8

QDs prepared at various synthesis temperatures. First, a monotonic and slow-slop increase in the absorbance of all samples somehow indicates the considerable influence of intra-gap energy levels on the absorption process. As can be seen, the absorption edge region for QDs prepared at 60 °C is around 540 nm, and no obvious peak related to the first excitonic absorption is observed. The absence of the first exciton absorption peak suggested that the CIS/ZnS QDs have a small exciton binding energy [23]. By plotting the Lnα versus $h\nu$, the curve fitting of its linear portion showed that the absorption edge of the CIS/ZnS QDs has the form of Urbach tail with the Urbach energy of about 120 meV. With a Stokes shift of 70 nm, the PL emission peak of CIS/ZnS QDs prepared at 60 °C is located near 611 nm with an FWHM of about 105 nm. The gradual increase in absorbance of samples, relatively high Urbach energy, large Stokes shift, and large FWHM value along with the results obtained from TSCPC decay curves provide reliable features about the significant involvement of the mid-gap states on optical properties of the present QDs. Similar trends also obtained for core/shell QDs prepared at other reaction temperatures. In addition, with increasing the reaction temperature, the absorption edge moves toward longer wavelengths, which can be due to the growth of CIS/ZnS QDs and the increase in their size (As demonstrated in Fig. 2C). This increase in the size of QDs is accompanied by a reduction in their

bandgap energy. Indeed, the bandgap energies calculated by Tauc relation [28] were 2.3, 2.15, and 2.10 eV for CIS/ZnS core/shell QDs prepared at temperatures of 60, 80, and 100 °C, respectively. The values estimated here are comparable with those reported by Wada et al. [29] and are still highly greater than that of CIS bulk structure. These results indicated that the main factor affecting the electronic properties of QDs is the quantum confinement effect. Finally, an increase at reaction temperature led to remarkable improvement in PL emission intensity (quantum yield), along with a red-shift in its peak position. The shift in emission wavelength from 612 nm to 641 nm is due to the size-driven change in band edge position and reduction of bandgap energy. Inset of Fig. 4A supports the results of PL spectra for refluxing temperature, as the prepared CIS/ZnS core/ shell QDs emit different colors from orange to red under UV irradiation. Nam et al. have attributed this red-shift in the emission peak position of their Cu-deficient CIS/ZnS QDs to the efficient contribution of sulfur and copper vacancy sites that acted as the radiative-recombination process [9]. They demonstrated that these defect states are more or less movable along with QD size, as their energy is near the band edge energies of the CIS host structure. There is also a remarkable increase in emission intensity, which can be illustrated as follows; Increase at reaction temperature leads to the growth of QDs, decrease in the surface-to-volume ratio, and
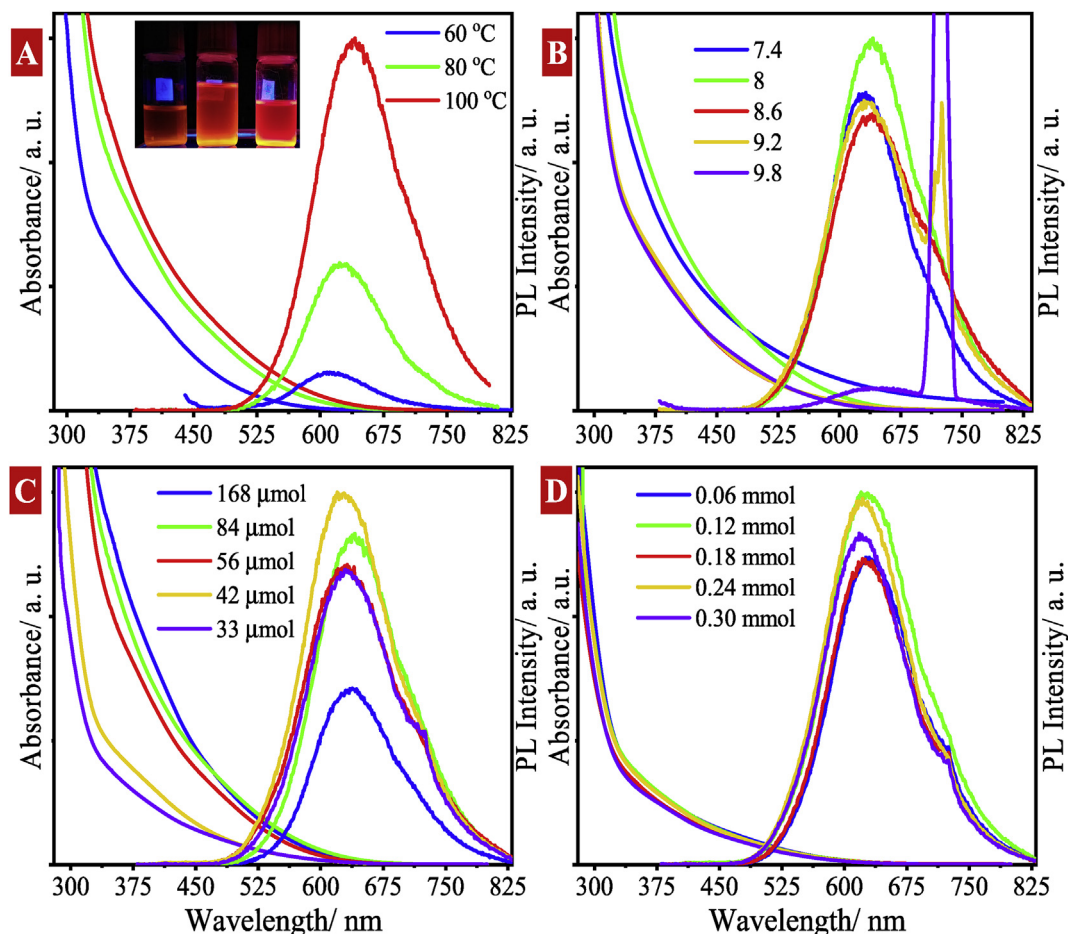
Fig. 4. The UV−Vis absorption and PL emission spectra ($\lambda_{exc} = 365$ nm) of CIS/ZnS QDs prepared at different, (A) reaction temperatures (Inset: A digital image of colloidal core/shell QDs under 365 nm/6 W irradiation), (B) solution pH, (C) concentration of core solution, and (D) concentration of shell solution.

subsequent reduction in the density of surface defects. In other words, higher reaction temperature results in lower band gap energy of CIS cores, providing more effective surface passivation by the ZnS shell with a wide bandgap. These surface defects usually dictate the non-radiative recombinations and show the fast decay rate character. Hence, better passivation decreases the non-radiative recombination possibility of carriers and enhances the emission intensity. The data reported for PL decay lifetimes demonstrate our assertion, because they exhibited a longer decay rate (through donor-acceptor levels) with an increase at the reaction temperature. The best PL emission QY was still 18%.

3.3.2. Effect of solution pH

The effect of solution pH on the absorption and PL emission spectra of the CIS/ZnS QDs was shown in Fig. 4B. As can be seen, an increase in pH value (during the preparation of the precursor solution) leads to the blue-shift in the absorption spectrum, and at the solution pH of 7.4, a broad/non-zero absorption tail is observed in the long-wavelengths region. However, samples prepared at pH = 8.6, 9.2, and 9.8 show exactly similar absorption spectra. The results recorded for PL emission spectra showed that the emission intensity completely quenched at pH = 9.8 (It should be pointed out that the intense/sudden increase in emission intensity for some of PL spectra is related to second harmonic generation of the $\lambda_{exc} = 365$ nm). This obvious decrease in emission intensity at pH of 9.8 might be ascribed to the formation of surface defects, which leads to the most probability of the nonradiative recombination

processes [30]. Furthermore, Mei et al. have reported similar results for decreasing emission intensity at high pH values in the synthesis of CIS/ZnS QDs [15]. They attributed this observation to the difficulty in forming the ZnS shell at high pH values, which results in poor passivation of surface defects and thus lower emission intensity. On the other hand, despite a significant change in the absorption spectra, the wavelength of the emission peaks kept unchanged. These important observations indicate that intra-gap energy levels play a key role in the recombination processes of the as-prepared QDs. The best PL emission QY of core/shell QDs at this step was 18%.

3.3.3. Effect of core and shell precursor solutions' concentration

In order to examine the effects of precursor's concentration on the optical properties of the as-synthesized QDs, the amounts of the core ([Cu + In]) and shell ([Zn]) precursors were changed. As shown in Fig. 4C, with a decrease in the amount of core precursors, the absorbance of CIS/ZnS QDs in the short wavelength region decreased. Since the value of absorbance cautiously indicates the concentration of QDs in the colloidal solution, a reduction in its value can be attributed to a decrease in the concentration of QDs [31]. Despite this, Lunz et al. attributed these effects to Förster resonant energy transfer (FRET) from smaller to larger QDs within the ensemble [32]. For as-prepared CIS/ZnS QDs, with increasing the concentration of core solution a non-linear trend at the emission intensity has occurred and the best result obtained at the amount of 42 µmol for the core precursor. There is also an overall

blue shift from 641 nm to 620 nm in 42 μmol of core precursor. The optimized PL emission QY of QDs at different core concentrations was ~23%.

As already shown, the presence of the ZnS shell has a meaningful effect on the PL characteristics of CIS QDs. In the next step, using an initial 42 μmol of the core precursor solution, at pH = 8 and refluxing temperature of 100 °C, the amount of utilized ZnS shell precursor was adjusted to different values (0.06, 0.12, 0.18, 0.24, and 0.30 mmol). As shown in Fig. 4D, all the absorption spectra are quite similar indicating that the amount of shell solution does not influence the absorption process of CIS/ZnS QDs. On the other hand, the highest intensity of PL emission was obtained for the QDs prepared using 0.12 mmol of shell precursor amount. Further increase in the amount of shell precursor resulted in a decrease in the emission intensity. The best PL emission QY calculated at this step was still near 23%.

3.3.4. Effect of precursors' feeding ratio

3.3.4.1. SC:In molar ratio. A vital factor governing the quality, stability, and dispersibility of QDs in colloidal solutions is the presence of capping or stabilizing agent molecules and their amounts. As shown in Fig. 5A, here, we found out that the presence of only one type of conventional thiol molecules (NAC) is not adequate to reach high-quality CIS/ZnS QDs. The SC is a long chain molecule with promising features in the preparation of such multi-component I-III-VI QDs [33,34]. Even at the low amount of SC (SC:In = 0.7:1), no emission signal was observed and a non-trivial absorbance

appeared at long-wavelengths. Indeed, at this molar ratio, the colloidal solution turned opaque and aggregation of QDs was clearly observed, indicating the necessity for utilizing SC at higher levels. It may control the comparative reactivity of Cu and In cations and provide a suitable situation for the growth of well-structured QDs. Nonetheless, the absorption spectra of CIS/ZnS QDs prepared with other amounts of SC are quite similar. The best PL emission intensity was obtained at SC:In feeding ratio of 1.4:1. The best PL emission QY of core/shell QDs at this step was ~24%.

3.3.4.2. NAC:In molar ratio. In the present study, in addition to SC, NAC thiol molecules were used to cap the surface of QDs. According to the results shown in Fig. 5B, all the absorption spectra are similar, indicating that the amount of NAC capping molecules does not influence the size and band edge position of CIS/ZnS QDs. Nonetheless, the colloidal CIS/ZnS QDs prepared at NAC:In molar ratio of 1.4:1 shows the highest emission intensity along with a small blue shift in the position of emission peak compared to low amounts of NAC (from 618 to 612 nm). After optimizing the NAC content, the PL QY was estimated again. It showed a slight increase to ~27%.

3.3.4.3. Cu:In molar ratio. The absorption and PL emission spectra of CIS/ZnS QDs prepared at different Cu:In feeding ratios (0.7:100, 3:100, 6:100, 12:100, and 18:100) were recorded, and have been shown in Fig. 5C. As can be seen, an increase in the copper amount (while indium amount remained constant) is accompanied by an obvious red-shift in the absorption spectrum and the absorption
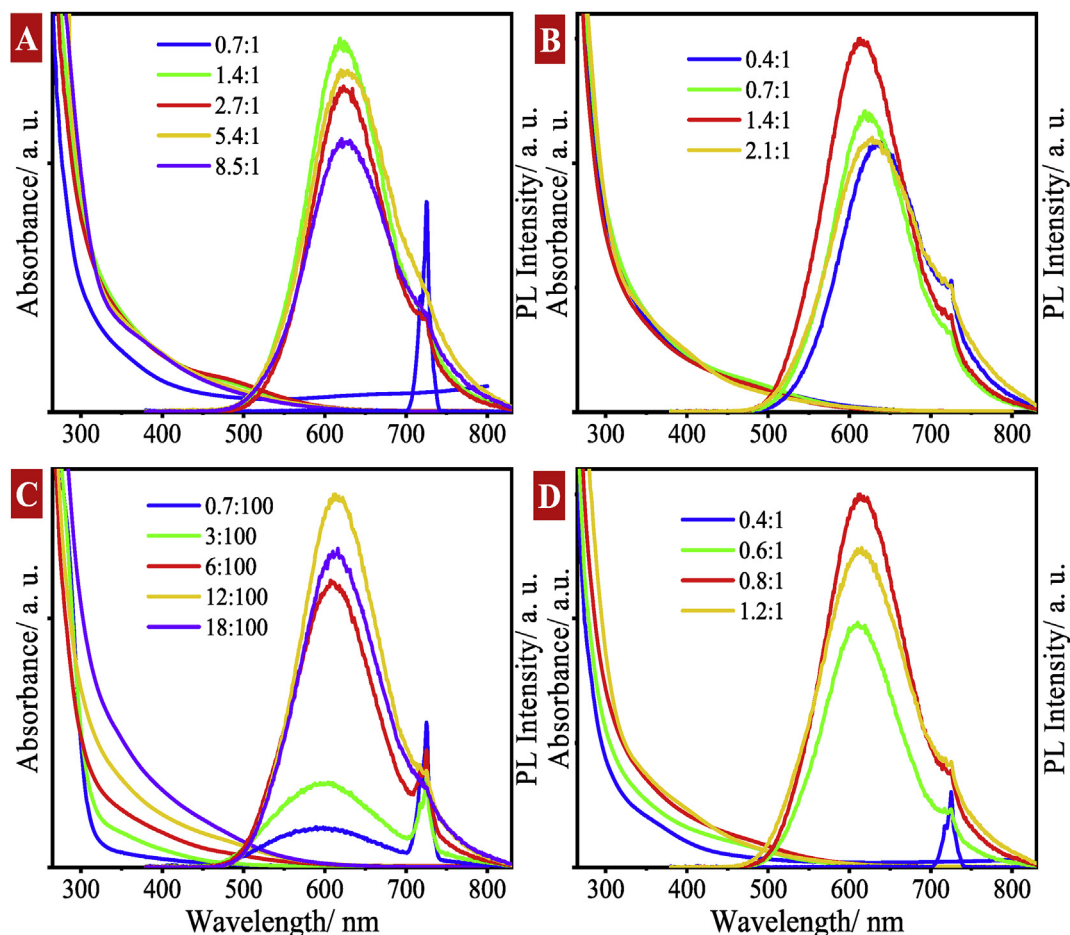

Fig. 5. The UV−Vis absorption and PL emission spectra (λ_{exc} = 365 nm) of CIS/ZnS QDs prepared at different feeding ratio of precursors; (A) SC:In, (B) NAC:In, (C) Cu:In, and (D) Na$_2$S:In.

edge wavelength. The calculation of the bandgap energy using Tauc's equation showed that with an increase in Cu:In molar ratio (from 0.7:100 to 18:100), the bandgap energy of the prepared samples is varied from 2.7 to 1.9 eV. This wide tunability in bandgap energy can be attributed to the alteration in the chemical composition of the as-prepared CIS multicomponent QDs. On the other hand, despite the high dependence of the intensity of the PL emission spectra on the increase in the Cu:In molar ratio, a gradual red-shift occurs at the position of the emission peaks from ~594 nm to ~616 nm [9]. These results imply the remarkable contribution of midgap donor-acceptor energy levels in radiative recombination processes. The PL quantum yield of as-prepared QDs increases up to 27% at Cu:In molar ratio of 12:100 and then decreased. In addition, regarding the low concentration of Cu ions the ICP-AES measurements were performed to give a better understanding of the exact Cu:In ratios in QDs' structure. The real amounts for Cu:In feeding
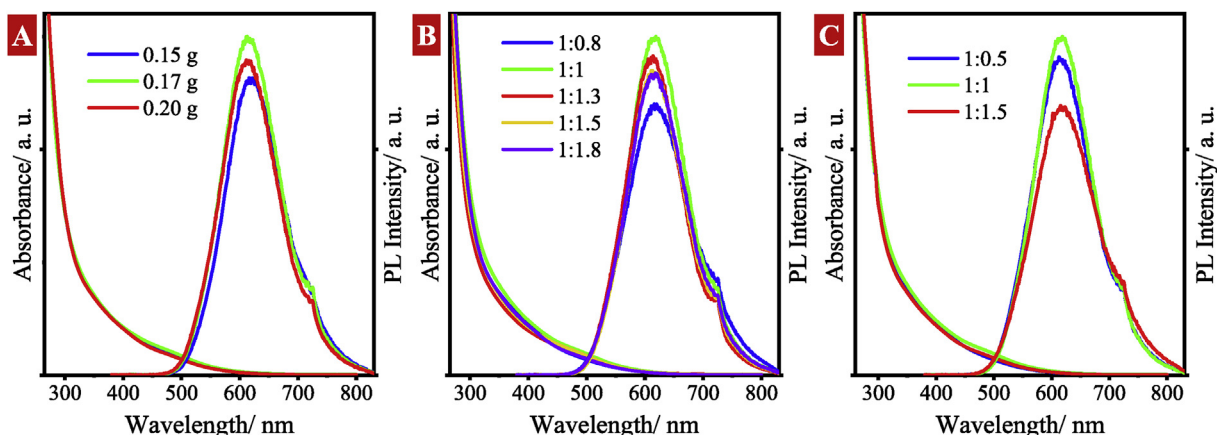

Fig. 6. The UV−Vis absorption and PL emission spectra (λ_{exc} = 365 nm) of CIS/ZnS QDs prepared at different; (A) Zn amount, (B) Zn:NAC, and (C) Zn:thiourea feeding ratio of precursors in shell solution.
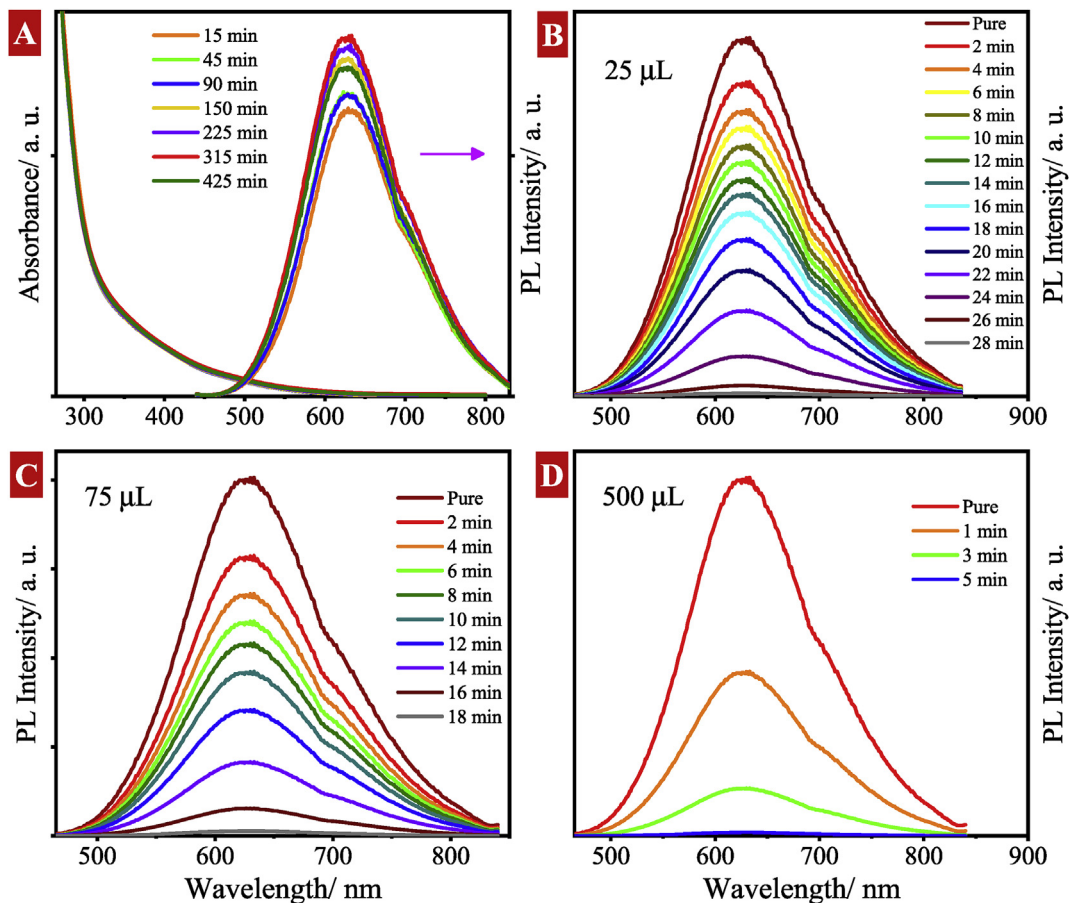

Fig. 7. (A) The UV−Vis absorption and PL emission spectra (λ_{exc} = 365 nm) of CIS/ZnS QDs prepared at different reaction times for ZnS overcoating. (B−D) Changes in PL intensity of the optimized QDs at different volumes of H$_2$O$_2$ solution; 25 μL, 75 μL, 500 μL.

ratios of 0.7:100, 3:100, 6:100, 12:100, and 18:100 were 0.51:99.49, 2.03:97.97, 4.84:95.16, 10.12:89.88, 15.64:84.36, respectively. As can be seen, the incorporated amount of Cu is slightly lower than the initial amount and increases with an increase in the Cu-to-In ratio.

3.3.4.4. Na_2S:In molar ratio. The presence of sufficient anion sites to create a well-structured lattice is always of great importance in the colloidal phase synthesis of QDs. Therefore, the effect of the Na_2S:In molar ratios on the optical properties of CIS/ZnS QDs was investigated (see Fig. 5D). There are two main observations. First, with increasing Na_2S content, the overall red-shift in absorption edge wavelengths is observed. It could be due to the change in the chemical composition of the CIS/ZnS QDs via the formation of Cu-rich QDs at a high molar ratio of Na_2S:In. Although there is an enormous difference in the solubility products of In_2S_3 ($K_{sp} = 5.8 \times 10^{-74}$) and CuS ($K_{sp} = 6.3 \times 10^{-36}$) [35], in a relatively large amount of Na_2S, the Cu cations can also react with S^{2-} ions and readily incorporated into the crystal structure of CIS/ZnS QDs. In the other words, at a specific molar ratio of Cu:In (12:100), an increase in the amount of Na_2S is accompanied by a more effective contribution of Cu cations in the lattice of CIS/ZnS QDs. This leads to a reduction in the bandgap energy and a red-shift in the absorption edge. Secondly, there is an obvious increase in the emission intensity with an increase in the amount of Na_2S. It could be due to the formation of more CIS/ZnS QDs at the large enough amounts of Na_2S. It is also clear that the lowest amount of sulfide ions results in a very weak emission peak, demonstrating the importance of high-enough amounts of anion sites presented in the lattice structure of CIS/ZnS QDs.

3.3.5. Effect of precursors' molar ratio in ZnS shell solution. The effect of precursors molar ratio used in ZnS shell solution on optical properties of CIS/ZnS QDs was also studied. The results have been shown in Fig. 6. As has been shown, the change in the amount of shell constituent precursor solution has no effect on the absorption spectrum, while the best PL emission results obtained at the Zn:NAC:thiourea molar ratio of 1:1:1. After evaluating the effects of Na_2S concentration and shell molar ratio, the maximum of PL QY was still 27%.

3.3.6. Effect of shell over-coating duration. The final optimization on the shell over-coating process was carried out by changing the duration of reaction time. Fig. 7A shows that an increase in the duration of the shelling process did not cause any change in the absorption spectra, while it accompanied with an enhancement in the emission intensity of the PL spectra, up to 315 min. The PL emission quantum efficiency of the final optimized sample is estimated to be about 30%, which is a very good value for aqueous-based I-III-VI QDs prepared at relatively low temperature and short reaction time.

3.3.7. Colloidal stabilities of QDs. The long-term stability of the fluorescent QDs in bio-imaging applications is of vital importance, which encourages researchers to concentrate on it. Therefore, after optimizing the optical properties of the as-synthesized CIS/ZnS core/shell QDs, their chemical stability was investigated. The stability test of the samples against chemical corrosion was performed by rapid adding 25, 75, and 500 μL of H_2O_2 stock solution (H_2O_2 solution 3%) to 2 mL of CIS/ZnS QDs solution. Fig. 7B, C, and 7D show that depending on the volume of H_2O_2 added, there are different trends in emission intensity of CIS/ZnS QDs. For 500 μL of H_2O_2 (which is a very high concentration relative to other reports [36,37]), the intensity of the emission peak reduced to zero after 5 min. While for 75 and 25 μL of H_2O_2 solution, the emission intensity decreased to zero after 18 and 28 min, respectively. These results

support the high stability of QDs in aqueous solution, indicating their suitability for real applications in biology.

4. Conclusions

In the present work, the utmost attention was paid to introduce a simple, versatile and cost-effective colloidal strategy for preparing aqueous-soluble, high quality and strongly luminescent CIS/ZnS QDs with low-toxicity character. NAC and SC were used as dual-stabilizing agents to make optically and chemically stable QDs with bright red emission. TEM image showed that the samples were composed of well-distributed small size QDs with a relatively spherical shape, which demonstrated the dominance of strong confinement regime on the charge carriers and optical properties of the QDs. The PL decay profiles proved the remarkable role of mid-gap levels in the recombination process. The optimization of experimental variables also showed their considerable effects on luminescent characteristics of CIS/ZnS QDs. It was found that without a ZnS shell layer, the bare CIS QDs have no luminescent emission. On the other hand, the reaction temperature, solution pH, the amounts of SC, Cu, and Na_2S have the major effects on the PL emission intensity of as-prepared samples. The results obtained in this work, highlight the great potential of the as-prepared CIS/ZnS core/shell QDs from both physicochemical and technological perspectives.

Declaration of competing interest

The authors declare that they have no known competing financial interests or personal relationships that could have appeared to influence the work reported in this paper.

CRediT authorship contribution statement

Nawzad Nadhim Jawhar: Data curation, Formal analysis, Investigation, Methodology, Resources, Software, Validation, Visualization. **Ehsan Soheyli:** Formal analysis, Data curation, Investigation, Methodology, Resources, Software, Validation, Visualization, Writing - original draft, Writing - review & editing. **Ahmet Faruk Yazici:** Formal analysis, Data curation, Investigation, Validation. **Evren Mutlugun:** Investigation, Validation, Methodology, Writing - review & editing. **Reza Sahraei:** Conceptualization, Funding acquisition, Investigation, Methodology, Project administration, Writing - original draft, Writing - review & editing.

References

[1] G. Xu, S. Zeng, B. Zhang, M.T. Swihart, K.T. Yong, P.N. Prasad, New generation cadmium-free quantum dots for biophotonics and nanomedicine, Chem. Rev. 116 (2016) 12234–12327, https://doi.org/10.1021/acs.chemrev.6b00290.

[2] J. Kolny-Olesiak, H. Weller, Synthesis and application of colloidal $CuInS_2$ semiconductor nanocrystals, ACS Appl. Mater. Interfaces 5 (2013) 12221–12237, https://doi.org/10.1021/am404084d.

[3] Q. Cai, Z. Liu, C. Han, Z. Tong, C. Ma, $CuInS_2/Sb_2S_3$ heterostructure modified with noble metal co-catalyst for efficient photoelectrochemical water splitting, J. Alloy. Comp. 795 (2019) 319–326, https://doi.org/10.1016/J.JALLCOM.2019.04.312.

[4] M. Sandroni, R. Gueret, K.D. Wegner, P. Reiss, J. Fortage, D. Aldakov, M.N. Collomb, Cadmium-free $CuInS_2$/ZnS quantum dots as efficient and robust photosensitizers in combination with a molecular catalyst for visible light-driven H_2 production in water, Energy Environ. Sci. 11 (2018) 1752–1761, https://doi.org/10.1039/c8ee00120k.

[5] L. Liu, H. Li, Z. Liu, Y.H. Xie, The conversion of $CuInS_2$/ZnS core/shell structure from type I to quasi-type II and the shell thickness-dependent solar cell performance, J. Colloid Interface Sci. 546 (2019) 276–284, https://doi.org/10.1016/j.jcis.2019.03.075.

[6] T. Chen, X. Hu, Y. Xu, L. Wang, W. Jiang, W. Jiang, Z. Xie, Hydrothermal synthesis of highly fluorescent Ag–In–S/ZnS core/shell quantum dots for white light-emitting diodes, J. Alloy. Comp. 804 (2019) 119–127, https://doi.org/10.1016/J.JALLCOM.2019.06.134.

[7] H.Y. Ueng, H.L. Hwang, The defect structure of CuInS$_2$. part I: intrinsic defects, J. Phys. Chem. Solids 50 (1989) 1297–1305, https://doi.org/10.1016/0022-3697(89)90403-4.

[8] A.D.P. Leach, J.E. Macdonald, Optoelectronic properties of CuInS$_2$ nanocrystals and their origin, J. Phys. Chem. Lett. 7 (2016) 572–583, https://doi.org/10.1021/acs.jpclett.5b02211.

[9] D.E. Nam, W.S. Song, H. Yang, Noninjection, one-pot synthesis of Cu-deficient CuInS$_2$/ZnS core/shell quantum dots and their fluorescent properties, J. Colloid Interface Sci. 361 (2011) 491–496, https://doi.org/10.1016/j.jcis.2011.05.058.

[10] A.S. Fuhr, H.J. Yun, N.S. Makarov, H. Li, H. McDaniel, V.I. Klimov, Light emission mechanisms in CuInS$_2$ quantum dots evaluated by spectral electrochemistry, ACS Photonics 4 (2017) 2425–2435, https://doi.org/10.1021/acsphotonics.7b00560.

[11] B. Chen, H. Zhong, W. Zhang, Z. Tan, Y. Li, C. Yu, T. Zhai, Y. Bando, S. Yang, B. Zou, Highly emissive and color-tunable CuInS$_2$-based colloidal semiconductor nanocrystals: off-stoichiometry effects and improved electroluminescence performance, Adv. Funct. Mater. 22 (2012) 2081–2088, https://doi.org/10.1002/adfm.201102496.

[12] L. Jing, S.V. Kershaw, Y. Li, X. Huang, Y. Li, A.L. Rogach, M. Gao, Aqueous based semiconductor nanocrystals, Chem. Rev. 116 (2016) 10623–10730, https://doi.org/10.1021/acs.chemrev.6b00041.

[13] B. Zhang, Y. Wang, C. Yang, S. Hu, Y. Gao, Y. Zhang, Y. Wang, H.V. Demir, L. Liu, K.T. Yong, The composition effect on the optical properties of aqueous synthesized Cu–In–S and Zn–Cu–In–S quantum dot nanocrystals, Phys. Chem. Chem. Phys. 17 (2015) 25133–25141, https://doi.org/10.1039/C5CP03312H.

[14] Y. Chen, S. Li, L. Huang, D. Pan, Low-cost and gram-scale synthesis of water-soluble Cu–In–S/ZnS core/shell quantum dots in an electric pressure cooker, Nanoscale 6 (2014) 1295–1298, https://doi.org/10.1039/C3NR05014A.

[15] S. Mei, J. Zhu, W. Yang, X. Wei, W. Zhang, Q. Chen, L. He, Y. Jiang, R. Guo, Tunable emission and morphology control of the Cu-In-S/ZnS quantum dots with dual stabilizer via microwave-assisted aqueous synthesis, J. Alloy. Comp. 729 (2017) 1–8, https://doi.org/10.1016/J.JALLCOM.2017.09.133.

[16] L. Jia, Y. Wang, Q. Nie, B. Liu, E. Liu, X. Hu, J. Fan, Aqueous-synthesis of CuInS$_2$ core and CuInS$_2$/ZnS core/shell quantum dots and their optical properties, Mater. Lett. 200 (2017) 27–30, https://doi.org/10.1016/J.MATLET.2017.04.082.

[17] J. Zhang, W. Sun, L. Yin, X. Miao, D. Zhang, One-pot synthesis of hydrophilic CuInS$_2$ and CuInS 2-ZnS colloidal quantum dots, J. Mater. Chem. C 2 (2014) 4812–4817, https://doi.org/10.1039/c3tc32564d.

[18] Y. Chen, S. Li, L. Huang, D. Pan, Green and facile synthesis of water-soluble Cu-In-S/ZnS core/shell quantum dots, Inorg. Chem. 52 (2013) 7819–7821, https://doi.org/10.1021/ic400083w.

[19] C. Neela Mohan, V. Renuga, Exploration of dopant and surface passivation on optical and morphological properties of AgInS2 nanocrystals, J. Alloy. Comp. 787 (2019) 972–981, https://doi.org/10.1016/J.JALLCOM.2019.02.191.

[20] X. Long, F. Zhang, Y. He, S. Hou, B. Zhang, G. Zou, Promising anodic electro-chemiluminescence of nontoxic core/shell CuInS$_2$/ZnS nanocrystals in aqueous medium and its biosensing application, Anal. Chem. 90 (2018) 3563–3569, https://doi.org/10.1021/acs.analchem.8b00006.

[21] R. Sahraei, E. Soheyli, Z. Faraji, M. Soleiman-Beigi, Facile, one-pot and scalable synthesis of highly emissive aqueous-based Ag,Ni:ZnCdS/ZnS core/shell quantum dots with high chemical and optical stability, Nanotechnology 28 (2017) 475604, https://doi.org/10.1088/1361-6528/aa92b2.

[22] O. Yarema, M. Yarema, V. Wood, Tuning the composition of multicomponent semiconductor nanocrystals: the case of I-III-VI materials, Chem. Mater. 30 (2018) 1446–1461, https://doi.org/10.1021/acs.chemmater.7b04710.

[23] R. Yan, W. Zhang, W. Wu, X. Dong, Q. Wang, J. Fan, Optical spectroscopy reveals transition of CuInS$_2$/ZnS to Cu$_x$Zn$_{1-x}$InS$_2$/ZnS:Cu alloyed quantum dots with resultant double-defect luminescence, Apl. Mater. 4 (2016) 126101, https://doi.org/10.1063/1.4971353.

[24] T. Chevallier, G. Le Blevennec, F. Chandezon, Photoluminescence properties of AgInS$_2$-ZnS nanocrystals: the critical role of the surface, Nanoscale 8 (2016) 7612–7620, https://doi.org/10.1039/c5nr07082a.

[25] O. Stroyuk, A. Raevskaya, F. Spranger, O. Selyshchev, V. Dzhagan, S. Schulze, D.R.T. Zahn, A. Eychmüller, Origin and dynamics of highly efficient broadband photoluminescence of aqueous glutathione-capped size-selected Ag–In–S quantum dots, J. Phys. Chem. C 122 (2018) 13648–13658, https://doi.org/10.1021/acs.jpcc.8b00106.

[26] A.S. Fuhr, P. Sautet, A.N. Alexandrova, Heterogeneity in local chemical bonding explains spectral broadening in quantum dots with Cu impurities, J. Phys. Chem. C 123 (2019) 5705–5713, https://doi.org/10.1021/acs.jpcc.8b12023.

[27] S.S. Chetty, S. Praneetha, S. Basu, C. Sachidanandan, A.V. Murugan, Sustainable, rapid synthesis of bright-luminescent CuInS$_2$-ZnS: multistage nano-xenotoxicity assessment and intravital fluorescence bio-imaging in zebrafish-embryos, Sci. Rep. 6 (2016) 26078, https://doi.org/10.1038/srep26078.

[28] E. Soheyli, R. Sahraei, G. Nabiyouni, Aqueous based synthesis of N-acetyl-L-cysteine capped ZnSe nanocrystals with intense blue emission, Opt. Mater. 60 (2016) 564–570, https://doi.org/10.1016/j.optmat.2016.07.025.

[29] C. Wada, Y. Iso, T. Isobe, H. Sasaki, Preparation and photoluminescence properties of yellow-emitting CuInS$_2$/ZnS quantum dots embedded in TMAS-derived silica, RSC Adv. 7 (2017) 7936–7943, https://doi.org/10.1039/c7ra00081b.

[30] J.Y. Chang, G.R. Chen, J.D. Li, Synthesis of magnetofluorescence Gd-doped CuInS$_2$/ZnS quantum dots with enhanced longitudinal relaxivity, Phys. Chem. Chem. Phys. 18 (2016) 7132–7140, https://doi.org/10.1039/c5cp07063e.

[31] Y. Wang, C. Wang, S. Xu, H. Shao, Y. Jiang, F. Bo, Z. Wang, Y. Cui, One-pot synthesis of multicolor MnSe:ZnSe nanocrystals, J. Colloid Interface Sci. 415 (2014) 7–12, https://doi.org/10.1016/j.jcis.2013.10.009.

[32] M. Lunz, A.L. Bradley, W.Y. Chen, V.A. Gerard, S.J. Byrne, Y.K. Gun'Ko, V. Lesnyak, N. Gaponik, Influence of quantum dot concentration on Förster resonant energy transfer in monodispersed nanocrystal quantum dot monolayers, Phys. Rev. B 81 (2010) 205316, https://doi.org/10.1103/PhysRevB.81.205316.

[33] X.B. Fan, S. Yu, F. Zhan, Z.J. Li, Y.J. Gao, X.B. Li, L.P. Zhang, Y. Tao, C.H. Tung, L.Z. Wu, Nonstoichiometric Cu$_x$In$_y$S quantum dots for efficient photocatalytic hydrogen evolution, ChemSusChem 10 (2017) 4833–4838, https://doi.org/10.1002/cssc.201701950.

[34] Y. Xu, T. Chen, X. Hu, W. Jiang, L. Wang, W. Jiang, J. Liu, The off-stoichiometry effect on the optical properties of water-soluble copper indium zinc sulfide quantum dots, J. Colloid Interface Sci. 496 (2017) 479–486, https://doi.org/10.1016/j.jcis.2017.02.049.

[35] C.C. Chang, C.J. Liang, K.W. Cheng, Physical properties and photoresponse of Cu-Ag-In-S semiconductor electrodes created using chemical bath deposition, Sol. Energy Mater. Sol. Cells 93 (2009) 1427–1434, https://doi.org/10.1016/j.solmat.2009.03.014.

[36] T. Xuan, S. Wang, X. Wang, J. Liu, J. Chen, H. Li, L. Pan, Z. Sun, Single-step noninjection synthesis of highly luminescent water soluble Cu$^+$ doped CdS quantum dots: application as bio-imaging agents, Chem. Commun. 49 (2013) 9045, https://doi.org/10.1039/c3cc44601h.

[37] E. Soheyli, R. Sahraei, G. Nabiyouni, F. Nazari, R. Tabaraki, B. Ghaemi, Luminescent, low-toxic and stable gradient-alloyed Fe:ZnSe(S)@ZnSe(S) core:shell quantum dots as a sensitive fluorescent sensor for lead ions, Nanotechnology 29 (2018) 445602, https://doi.org/10.1088/1361-6528/aada29.